

DRAFT VERSION FEBRUARY 27, 2026

Typeset using L^AT_EX **manuscript** style in AASTeX7.0.1

KMT-2024-BLG-3237: Another Free-floating Planet Candidate with Angular Einstein Radius Measurement

TANAGODCHAPORN INYANYA,^{1,2} YOUN KIL JUNG,^{1,2} HONGJING YANG,³ KYU-HA HWANG,¹
ANDREW GOULD,⁴ MICHAEL D. ALBROW,⁵ SUN-JU CHUNG,¹ CHEONGHO HAN,⁶ YOON-HYUN RYU,¹
IN-GU SHIN,⁷ YOSSI SHVARTZVALD,⁸ JENNIFER C. YEE,⁹ WEICHENG ZANG,³ DONG-JIN KIM,¹
CHUNG-UK LEE,¹ AND BYEONG-GON PARK¹

¹*Korea Astronomy and Space Science Institute, Daejeon 34055, Republic of Korea*

²*National University of Science and Technology (UST), Daejeon 34113, Republic of Korea*

³*Department of Astronomy, Westlake University, Hangzhou 310030, Zhejiang Province, China*

⁴*Department of Astronomy, Ohio State University, 140 W. 18th Ave., Columbus, OH 43210, USA*

⁵*University of Canterbury, School of Physical and Chemical Sciences, Private Bag 4800, Christchurch 8020, New Zealand*

⁶*Department of Physics, Chungbuk National University, Cheongju 28644, Republic of Korea*

⁷*School of Science, Westlake University, Hangzhou, Zhejiang 310030, China*

⁸*Department of Particle Physics and Astrophysics, Weizmann Institute of Science, Rehovot 7610001, Israel*

⁹*Center for Astrophysics | Harvard & Smithsonian, 60 Garden St., Cambridge, MA 02138, USA*

ABSTRACT

Planet formation theories suggest the presence of free-floating planets (FFPs) that are ejected from their formation sites. While these planets emit very little light, they can be identified through gravitational microlensing. Here, we report the discovery of a FFP candidate in the microlensing event KMT-2024-BLG-3237. The observed light curve exhibits strong finite-source effects characterized by a small amplitude ($\lesssim 0.9$ mag) and a short timescale ($\lesssim 3$ days). The analysis yields an Einstein timescale of $t_E = 0.54 \pm$

Corresponding author: Youn Kil Jung
ykjung21@kasi.re.kr

arXiv:2602.22709v1 [astro-ph.EP] 26 Feb 2026

0.02 days and an angular Einstein radius of $\theta_E = 6.30 \pm 0.48 \mu\text{as}$. The measurements make it possible to estimate the lens mass as $M \simeq 102 M_\oplus (\pi_{\text{rel}}/16 \mu\text{as})^{-1}$, where π_{rel} is the relative lens-source parallax. Depending on the unknown π_{rel} , the lens could be a Neptune-mass planet ($\pi_{\text{rel}} \simeq 0.1 \text{ mas}$) or a Saturn-mass planet ($\pi_{\text{rel}} \simeq 16 \mu\text{as}$). A Bayesian analysis yields the lens mass $M = 67.3^{+103.2}_{-42.5} M_\oplus$ and the lens distance $D_L = 7.34^{+0.96}_{-2.11} \text{ kpc}$. This lens is the eleventh isolated microlens with a measurement of $\theta_E < 10 \mu\text{as}$. We find that additional searches for possible signatures of a lens host do not show significant evidence for the host.

Keywords: gravitational microlensing exoplanet detection

1. INTRODUCTION

Free-floating planets (FFPs) are substellar objects with planetary masses, which are not gravitationally attached to any host star. These substellar objects can be formed, like stars, through the collapse and fragmentation of gas clouds (e.g., [Luhman 2012](#)). It is suggested that the minimum mass of the FFPs formed by this process ranges from ~ 1 to $\sim 10 M_J$ (e.g., [Whitworth & Stamatellos 2006](#); [Luhman 2012](#)). FFPs can also be formed in protoplanetary disks around stars, like ordinary planets, and then be ejected through various mechanisms. These include planet–planet scattering (e.g., [Rasio & Ford 1996](#)), dynamical interactions with stars in multiple-star systems (e.g., [Kaib et al. 2013](#)), stellar flybys (e.g., [Malmberg et al. 2011](#)), or orbital disruption caused by the host star’s evolution beyond the main sequence phase (e.g., [Veras & Raymond 2012](#)).

Considering that different FFP formation scenarios predict different mass distributions of FFPs, understanding their origins requires a statistical characterization of the FFP population across a broad mass range, from terrestrial to Jovian masses. Many nearby high-mass ($M \gtrsim M_J$) FFP candidates have been detected through high-resolution direct imaging (e.g., [Pearson & McCaughrean 2023](#)). However, low-mass FFPs ($M < M_J$) are rarely detected by the direct imaging method, as they remain below the brightness limits of currently available telescopes. In contrast, gravitational microlensing does not rely on the brightness of FFPs, and thus the microlensing method can pro-

vide a unique capability to detect FFPs down to terrestrial- (or even dwarf-planet-) mass objects (Gould et al. 2021, 2024).

The microlensing method observes the light from a distant source star, which is distorted and magnified by the gravitational field of a lensing object. A key observable in a microlensing event is the Einstein timescale, t_E , which relies on the relative lens-source (parallax, proper motion), $(\pi_{\text{rel}}, \mu_{\text{rel}})$, and the angular Einstein radius, θ_E , i.e.,

$$t_E = \frac{\theta_E}{\mu_{\text{rel}}}, \quad \theta_E \equiv \sqrt{\kappa M \pi_{\text{rel}}}, \quad \pi_{\text{rel}} = \text{au} \left(\frac{1}{D_L} - \frac{1}{D_S} \right), \quad (1)$$

where $\kappa \equiv 4G/(c^2 \text{ au}) = 8.14 \text{ mas } M_\odot^{-1}$ and M is the lens mass. Here, D_L and D_S are, respectively, the lens and the source distances. As $t_E \propto M^{1/2}$, it is expected that Einstein timescales due to FFPs are very short:

$$t_E = 0.8 \text{ days} \left(\frac{M}{1 M_J} \right)^{1/2} \left(\frac{\pi_{\text{rel}}}{16 \mu\text{as}} \right)^{1/2} \left(\frac{\mu_{\text{rel}}}{5 \text{ mas yr}^{-1}} \right)^{-1}. \quad (2)$$

We expect $t_E \simeq 0.8$ days for a Jupiter-mass lens, assuming typical values of $\pi_{\text{rel}} = 16 \mu\text{as}$ and $\mu_{\text{rel}} = 5 \text{ mas yr}^{-1}$, which correspond to typical events generated by lenses in the Galactic bulge. However, a secure lens-mass determination requires the measurements of both μ_{rel} and π_{rel} .

In the cases for which the lens closely approaches or transits the source, the source size affects the microlensing light curve (Gould 1994; Nemiroff & Wickramasinghe 1994; Witt & Mao 1994). For microlensing events that exhibit such finite-source effects, one can measure θ_E based on the detection of the normalized source radius $\rho = \theta_*/\theta_E$. Here, θ_* is the angular source radius. The θ_E measurement then enables us to estimate the lens mass with better accuracy, as it partially resolves the three-way degeneracy in t_E by eliminating μ_{rel} as an unknown parameter:

$$M = \frac{\theta_E^2}{\kappa \pi_{\text{rel}}} = 0.16 M_J \left(\frac{\theta_E}{5 \mu\text{as}} \right)^2 \left(\frac{\pi_{\text{rel}}}{16 \mu\text{as}} \right)^{-1}. \quad (3)$$

Finite-source effects can be strong for planetary-lens events, as their Einstein radii are comparable to the angular radii of sources, i.e., $\rho \approx 1$ (Bennett & Rhie 1996). In addition, if $\rho > 1$, strong finite-source effects increase the duration of events, which makes it possible to take more observations at a fixed cadence. This makes short-duration finite-source/point-lens (FSPL) events on giant-source stars

easier to detect than those on dwarf-source stars or short-duration point-source/point-lens (PSPL) events. Hence, one would expect that an efficient way to identify FFP candidates is to observe giant-source microlensing events (Kim et al. 2021; Gould et al. 2022; Koshimoto et al. 2023).

To resolve the $(M, \pi_{\text{rel}}, \mu_{\text{rel}})$ degeneracy requires one additional observable. This is the microlens parallax π_{E} , which is related to the lens mass and the relative parallax by (Gould 2000)

$$M = \frac{\theta_{\text{E}}}{\kappa\pi_{\text{E}}}; \quad \pi_{\text{E}} = \frac{\pi_{\text{rel}}}{\theta_{\text{E}}}. \quad (4)$$

The microlens parallax can be measured using the orbital acceleration of Earth (Gould 1992). However, this approach is challenging for FFP events due to their short timescales (Gould & Yee 2013). The alternative way to measure the parallax is to use simultaneous observations from two widely separated (ground- and space-based) observatories (Refsdal 1966). For example, the *Spitzer* telescope carried out microlensing observations with ground-based telescopes during the *Spitzer* microlensing campaign (Gould et al. 2013, 2014, 2015a,b, 2016, 2018). These observations made it possible to detect microlens parallaxes for a large number of single- and binary-lens events, including bound-planet systems (e.g., Udalski et al. 2015; Yee et al. 2015; Shvartzvald et al. 2017; Gould et al. 2020). The *Kepler* observations from the K2 Campaign 9 survey also provided π_{E} measurements for several events (e.g., Henderson et al. 2016; Zhu et al. 2017; Zang et al. 2018). Although parallax measurements of FFP events from these surveys were not reported, Ban (2020) showed that based on space-based parallax simulations, ground- and space-based telescopes could enable parallax measurements for FFPs down to $\sim 0.5 M_{\oplus}$ mass objects.

To date, ten short-timescale FSPL events have been reported (Mróz et al. 2018, 2019a, 2020a,b; Kim et al. 2021; Ryu et al. 2021; Koshimoto et al. 2023; Jung et al. 2024; Kapusta et al. 2025). All of these are characterized by $t_{\text{E}} < 2$ days and $\theta_{\text{E}} < 10 \mu\text{as}$, the latter of which is a useful threshold for planetary-mass lenses (Gould et al. 2022). These measurements imply that the lenses are either FFPs or wide-orbit ($\gtrsim 10$ au) planets, as microlensing observations alone cannot exclude the possibility of a distant host star (e.g., Clanton & Gaudi 2017). If these planetary-mass lenses are real FFPs, statistical studies (Gould et al. 2022; Sumi et al. 2023) suggest that unbound planets are

more common than wide-orbit planets and/or stellar objects. [Yee & Kenyon \(2025\)](#) have shown that, regardless of whether they are bound or free-floating, this population places interesting constraints on wide-orbit planet populations.

Here, we present the discovery of another FFP candidate identified in the microlensing event KMT-2024-BLG-3237, with measurements of $t_E \simeq 0.54$ days and $\theta_E \simeq 6.3 \mu\text{as}$. The lens magnified a giant source star with $\theta_* \simeq 6.42 \mu\text{as}$, located in the Galactic bulge.

2. OBSERVATIONS

KMT-2024-BLG-3237 occurred at (R.A., decl.)_{J2000} = (17:50:31.23, -32:15:48.89) [$(l, b) = (-2^\circ 31', -2^\circ 62')$]. This event was discovered by the Korea Microlensing Telescope Network (KMTNet; [Kim et al. 2016](#)), which consists of three 1.6 m telescopes equipped with $2^\circ \times 2^\circ$ cameras. The KMTNet telescopes are distributed at the South African Astronomical Observatory (KMST), the Cerro Tololo Inter-American Observatory (KMTC), and the Siding Spring Observatory (KMTA). The event was observed in the overlap region of KMTNet BLG41 and BLG22 fields, with cadences of $\Gamma = 2 \text{ hr}^{-1}$ for BLG41 and $\Gamma = 1 \text{ hr}^{-1}$ for BLG22, which combine to a total cadence of $\Gamma = 3 \text{ hr}^{-1}$. KMTNet observations were mainly taken in the Cousins I band, but after every 10th I -band observation, there was one observation in the Johnson V band. These observations were initially processed using the pySIS pipeline ([Albrow et al. 2009](#)), which was developed based on the Difference Image Analysis (DIA; [Tomaney & Crofts 1996](#); [Alard & Lupton 1998](#)).

KMT-2024-BLG-3237 was first identified in 2025 February through the KMTNet EventFinder package ([Kim et al. 2018](#)). The event, which showed deviations that would be indicative of FSPL events, was immediately recognized as an FFP candidate during the inspection of events found by the package. For the light-curve analysis, we then reprocessed the data sets using the refined pySIS pipeline ([Yang et al. 2024](#)).

Microlensing experience shows that the error bars measured from photometry pipelines are monotonically connected to the true errors, but the transformation from measured to true errors varies between events and/or between observatories. To address this effect, we rescale the error bars based

on the procedure presented in [Yee et al. \(2012\)](#). We use the formula

$$\sigma' = k\sqrt{\sigma_0^2 + (e_{\min})^2}, \quad (5)$$

where (k, e_{\min}) are the scaling parameters and σ_0 is the error measured from the pipeline. For each data set, we choose e_{\min} to make the cumulative χ^2 distribution ordered by source magnification linear. We next rescale the errors using k to make χ^2/dof unity. We note that this renormalization process is carried out based on the FSPL model.

3. LIGHT CURVE ANALYSIS

As shown in [Figure 1](#), the observed light curve exhibits deviations from a standard PSPL model, which is described by three geometric parameters (t_0, u_0, t_E) . Here, t_0 is the time of maximum magnification and u_0 is the lens-source separation at t_0 (normalized to θ_E), i.e., the impact parameter. Such deviations can be described by the FSPL model, which requires an additional fitting parameter ρ . For each observatory, we consider two flux parameters, (f_S, f_B) , to describe the source flux and any blended flux, respectively. The observed flux $F(t)$ is then given by

$$F(t) = f_S A(t) + f_B, \quad (6)$$

where $A(t)$ is the time-dependent lensing magnification. With these parameters, we fit the FSPL model to the data using the Markov Chain Monte Carlo (MCMC) technique. In this modeling, we utilize the inverse ray shooting method to calculate the finite-source magnification. To describe the source surface brightness profile, we also consider a linear limb-darkening model, i.e.,

$$\frac{S_\lambda}{\overline{S}_\lambda} = 1 - \Gamma_\lambda \left(1 - \frac{3}{2} \cos \theta\right), \quad (7)$$

where $\overline{S}_\lambda = F_{S,\lambda}/\pi\theta_*^2$ is the mean source surface brightness, $F_{S,\lambda}$ is the total source flux, Γ_λ is the limb-darkening coefficient, λ is the passband, and θ is the angular position on the source from its center. To find the coefficient Γ_λ , we use the linear limb-darkening model of [Claret \(2000\)](#), which is based on the intensity profile of a star, and use the relation $\Gamma_\lambda = 2u_\lambda/(3 - u_\lambda)$ ([Albrow et al. 2001](#)), where u_λ is the limb-darkening coefficient of [Claret \(2000\)](#) model. We adopt $\Gamma_I = 0.53$ based on the clump giant source estimated in [Section 4](#).

As listed in Table 1, we test two FSPL models: one with f_B as a variable and the other with f_B held fixed at zero ($f_B = 0$). We note that we adopt the KMTS BLG41 (KMTS41) as the representative observatory for the flux measurements, because this observatory densely covers the ascending and descending parts of the light curve, which enables us to precisely constrain the flux parameters. We find that both models give consistent results within 1σ , with a minor χ^2 difference of $\Delta\chi^2 = 0.7$. That is, the χ^2 difference is in the range of statistical noise. As discussed by Park et al. (2004), the negative blending in the free f_B model can be caused by low-level unseen systematics and/or statistical noise in the data. In addition, Mróz et al. (2019b) discussed that the distribution of blending fractions, $\eta = f_B/(f_S + f_B)$, of red giant stars is bimodal with values centering near 0 and 1. This implies that the observed flux is either dominated by the source ($\eta \sim 0$) or by the blended light ($\eta \sim 1$). Because our results are consistent with $\eta \sim 0$ and because the source position measured from difference images is closely aligned to the baseline object position [$\Delta(x, y) = (x, y)_S - (x, y)_{\text{base}} = (-0.007, 0.011)$ pixels $\simeq (-2.8, 4.4)$ mas], we adopt the $f_B = 0$ model as the preferred solution.

4. PHYSICAL PARAMETERS

4.1. Source Star

The ρ measurement enables us to infer $\theta_E = \theta_*/\rho$. Typically, one can measure θ_* based on the source flux measurements in two different passbands within the same photometric system. However, this method is not viable for the current case because we lack V -band images taken during the event. As an alternative, we adopt the color and magnitude of the baseline object as those of the source because our results show the absence of evidence for the blended flux (see Table 1) and because the I -band source magnitude $I_S = 18.26$ (inferred from the fitted source flux $f_S = 0.785$) is consistent with that of the baseline object $I_{\text{base}} = 18.26 \pm 0.02$. Here, the source magnitude is given by $I_S = 18 - 2.5 \log f_S$.

We estimate θ_* using the standard method of Yoo et al. (2004). We first make the color-magnitude diagram (CMD) with the KMTS41 observations, which includes nearby stars within $4'$ of the event (see Figure 2). In this CMD, the baseline object position is $(V - I, I)_{\text{base}} = (3.42 \pm 0.09, 18.26 \pm 0.02)$.

As described above, we adopt this measurement as the source position: $(V - I, I)_S = (V - I, I)_{\text{base}}$. We also find the giant clump (GC) position as $(V - I, I)_{\text{GC}} = (3.35 \pm 0.02, 18.33 \pm 0.02)$. The source offset from the GC is then $\Delta(V - I, I) = (0.07 \pm 0.09, -0.07 \pm 0.02)$. We next adopt the dereddened GC position as $(V - I, I)_{\text{GC},0} = (1.06, 14.56)$ from the measurements of [Nataf et al. \(2013\)](#) and [Bensby et al. \(2013\)](#), respectively. The dereddened source position is then

$$(V - I, I)_{S,0} = \Delta(V - I, I) + (V - I, I)_{\text{GC},0} = (1.13 \pm 0.10, 14.50 \pm 0.03), \quad (8)$$

which indicates that the lensed source is a K1- or K2-type red giant.

Due to heavy extinction along the line of sight, however, the uncertainty in the $(V - I)_S$ measurement is relatively large. To find a more precise estimate for the source color, we conduct an additional $(J - H, J)$ CMD analysis using the catalogue from the VISTA Variables in the Via Lactea (VVV) survey ([Minniti et al. 2023](#)). From this, we find $(J - H, J)_S = (1.13 \pm 0.04, 15.04 \pm 0.03)$ and $(J - H, J)_{\text{GC}} = (1.09 \pm 0.01, 15.07 \pm 0.01)$ (see Figure 2). The source offset from the GC is $\Delta(J - H, J) = (0.04 \pm 0.04, -0.03 \pm 0.03)$. We next convert $(V - I, I)_{\text{GC},0} = (1.06, 14.56)$ to $(J - H, J)_{\text{GC},0} = (0.57, 13.84)$ using the [Bessell & Brett \(1988\)](#) color-color relations. The dereddened source position is then $(J - H, J)_{S,0} = (0.61 \pm 0.04, 13.81 \pm 0.03)$. Finally, we convert $(J - H, J)_{S,0}$ to $(V - I, I)_{S,0}$ using the same color-color relations, which yields $(V - I, I)_{S,0} = (1.13 \pm 0.04, 14.49 \pm 0.03)$. We find that the KMTS41 and VVV source color measurements are consistent with each other, but the latter is more tightly constrained. Therefore, we use the VVV color to determine θ_* .

We then convert $(V - I, I)_{S,0}$ to $(V - K, K)_{S,0}$ using again the [Bessell & Brett \(1988\)](#) relations. Based on the the color-surface brightness relations from [Kervella et al. \(2004\)](#), we subsequently estimate the angular source radius as

$$\theta_* = 6.42 \pm 0.45 \mu\text{as}, \quad (9)$$

where we add a quadratic 5% error to the θ_* measurement to account for systematic errors and our assumption that $f_B = 0$. We find

$$\theta_E = 6.30 \pm 0.48 \mu\text{as}, \quad \mu_{\text{rel}} = 4.29 \pm 0.33 \text{ mas yr}^{-1}. \quad (10)$$

It is worthwhile to note that the source color is estimated from the baseline object based on our assumption that $f_B = 0$. If there is substantial blending (contrary to our assumption), the color could be incorrectly estimated, which in turn would affect the θ_E measurement.

4.2. Proper motion of the Source

Our results show that the source is bright (as estimated above) and the blending associated with the event is negligible. In this case, one can adopt the proper motion of the baseline object derived by Gaia as that of the source (e.g., Jung et al. 2024). Figure 3 shows proper motions of stars in the vicinity of the event (within $6'$) from the third Gaia data release (DR3; Gaia Collaboration et al. 2023). We rotate the Gaia measurements to Galactic coordinates using the coordinate transformation from Bachelet et al. (2018). The red and blue dots represent red giant (bulge population) and main sequence (disk population) stars, respectively¹⁰. The source proper motion is then

$$\boldsymbol{\mu}_S(l, b) = (-8.14, 0.57) \pm (0.44, 0.51) \text{ mas yr}^{-1}. \quad (11)$$

Here, Gaia reports the renormalized unit weight error (RUWE) value for this measurement as $\text{RUWE} = 1.036$, which indicates that the measurement errors are consistent with the excess scatter of the data for the 5-parameter astrometric solution. That is, astrometric systematic effects have no significant impact on the measurement. From the μ_{rel} and $\boldsymbol{\mu}_S$ measurements, we find that the lens proper motion $\boldsymbol{\mu}_L = \boldsymbol{\mu}_S + \boldsymbol{\mu}_{\text{rel}}$ lies close to the black circle in Figure 3. This implies that $\boldsymbol{\mu}_L$ is compatible with either bulge or disk lenses.

4.3. Constraints on the host star

The light-curve analysis, including the measurements of $t_E \simeq 0.54$ days and $\theta_E \simeq 6.30 \mu\text{as}$, suggests that the lens of KMT-2024-BLG-3237 is an FFP candidate. However, it is also possible that the lens orbits a widely separated host star. In such a case, the host may produce weak anomalies in the light curve. We therefore investigate the event with the binary-lens/single-source (2L1S) interpretation.

¹⁰ We adopt the Gaia DR3 stars that satisfy the RP magnitude of $19.2 < RP < 12.0$ and the $(BP - RP)$ color of $0.8 < (BP - RP) < 2.8$ as the main-sequence stars, while we adopt the DR3 stars with $19.1 < RP < 13.5$ and $2.9 < (BP - RP) < 4.3$ as the red giant stars. In each population, we exclude the stars that have the RUWE measurements of $\text{RUWE} > 1.5$.

For the 2L1S analysis, we follow the method described in [Kim et al. \(2021\)](#). We extend the FSPL model to the 2L1S case by introducing three binary-lens parameters (s, q, α) , i.e., the projected planet-host separation, their mass ratio, and the angle between the direction of $\boldsymbol{\mu}_{\text{rel}}$ and the planet-host axis (source trajectory angle). Here, the parameters (u_0, t_E, s, ρ) are scaled to the Einstein radius corresponding to the binary lens. We adopt a coordinate system centered on the caustic generated by the planet (planetary caustic) in order that t_0 remains comparable to the FSPL solution listed in [Table 1](#). Because the binary-lens parameter space is non-linear, we first conducted a grid search over fixed (s, q) grids with several trial values of α , which are uniformly distributed on the unit circle. From this grid search, we identify two local minima. We refine these minima with additional MCMC runs, but this time with all fitting parameters are allowed to vary.

We find no 2L1S solutions that provide significant χ^2 improvement over the FSPL solution. As listed in [Table 2](#), we find two (Local A and B) 2L1S solutions. However, the measured (s, q, α) are weakly constrained for both solutions, and their χ^2 difference is just $\Delta\chi^2 = 5.3$. Compared to the adopted FSPL ($f_B = 0$) model, the best-fit Local B solution gives a low-level χ^2 improvement of $\Delta\chi^2 = 6.4$ with four additional degrees of freedom. Assuming Gaussian statistics, this improvement corresponds to a significance of $p = (1 + \Delta\chi^2/2) \exp(-\Delta\chi^2/2) = 18\%$. Similar to the FSPL solutions, the Local B solution exhibits the negative blending, and thus we additionally test the solution with $f_B = 0$. From this, we find that the two Local B solutions give consistent results within 1σ and their χ^2 difference is just $\Delta\chi^2 = 0.7$. For the Local A solution, the source encloses both the central and the planetary caustics, and the strong finite-source effects suppress the caustic signatures. In addition, this solution improves the fit by just $\Delta\chi^2 = 1.1$ over the adopted FSPL model. These imply that the Local A solution is basically identical to the FSPL model except with an additional object.

Given that the event shows no significant signals that would be indicative of the lens host, we place a constraint on the lower limit of the projected planet-host separation. Following the method of [Gaudi & Sackett \(2000\)](#), we build a grid in the (q, s, α) space, which consists of $61 \times 101 \times 37$ points that are uniformly distributed over $0 \leq \log q \leq 6$, $0 \leq \log s \leq 2$, and $0 \leq \alpha \leq 2\pi$. At each point, we fit the 2L1S model to the event using the MCMC with (q, s, α) held fixed and obtain the

goodness of the fit $\chi_{2\text{L1S}}^2$ to find the χ^2 difference between the model and the adopted FSPL solution, i.e., $\Delta\chi^2 = \chi_{2\text{L1S}}^2 - \chi_{\text{FSPL}}^2$. For each (q, s) pair, we then derive the detection probability of the host from the fraction of 2L1S models that satisfy $\Delta\chi^2 < \Delta\chi_{\text{thresh}}^2$. Here, we set the threshold value as $\Delta\chi_{\text{thresh}}^2 = 50$, given that the χ^2 improvement of the Local B model relative to the FSPL solution is just $\Delta\chi^2 = 6.4$ (see Tables 1 and 2).

We find that for putative hosts with $\log q > 1.9$, the 90% lower separation limit corresponds to $s = 1.8$ (see Figure 4). If we assume a $0.6 M_{\odot}$ host with $\pi_{\text{rel}} = 0.1$ mas (disk lens), the lower limit for the physical projected separation would be $a_{\perp} = s\theta_{\text{E,host}}D_{\text{L}} \sim 6$ au. If we assume a $0.6 M_{\odot}$ host with $\pi_{\text{rel}} = 16 \mu\text{as}$ (bulge lens), the lower limit would be $a_{\perp} \sim 4$ au.

5. DISCUSSION

KMT-2024-BLG-3237 is well explained by an FSPL model, which yields $t_{\text{E}} = 0.54 \pm 0.02$ days and $\theta_{\text{E}} = 6.30 \pm 0.48 \mu\text{as}$. The measurements suggest that the lensing object is an FFP candidate, even though the lens mass is not unambiguously derived:

$$M = 102 M_{\oplus} \left(\frac{16 \mu\text{as}}{\pi_{\text{rel}}} \right). \quad (12)$$

The lens could be a Neptune- to Saturn-mass planet, depending on the unknown π_{rel} . In principle, one can constrain the lens mass with the Bayesian approach, which is based on Galactic priors including mass functions (MFs), density profiles (DPs), and velocity distributions (VDs). For the MF, we adopt the 4-component power law model from Sumi et al. (2023), which incorporates planetary, substellar, and stellar components. For the DP and VD, we use the models presented in Jung et al. (2021). We then perform a Bayesian analysis with the measured constraints $(t_{\text{E}}, \theta_{\text{E}})$, following the procedure presented in Jung et al. (2018). The posterior distributions for M and D_{L} are shown in Figure 5. The median and 68% confidence intervals of the distributions are then

$$M = 67.3_{-42.5}^{+103.2} M_{\oplus}, \quad D_{\text{L}} = 7.34_{-2.11}^{+0.96} \text{ kpc}. \quad (13)$$

Our Bayesian results suggest that the lens would be a Saturn-like planet located in the bulge.

As with other FFP candidate events, we cannot rule out the existence of a widely separated host star. We applied 2L1S models to the event to investigate possible signals for the host, but found

that the fit improvement by the best-fit 2L1S model is only $\Delta\chi^2 = 6.4$. For typical events with $M_{\text{host}} = 0.6 M_{\odot}$ and $D_L = 4.5 \text{ kpc}$, we detected no significant evidence for the lens host within the planet-host projected distance of $a_{\perp} \sim 6 \text{ au}$.

If the lens hosts a star, the host can be identified through high-resolution follow-up imaging. For KMT-2024-BLG-3237, however, the detection probability for possible hosts with current telescopes would be very low, due to the relatively bright source of $K_S \simeq 13.02$. Recently, Mróz et al. (2024) carried out follow-up observations using Keck adaptive optics, together with sensitivity simulations for putative hosts, and calculated the detection probability of possible hosts for the six PSPL FFP candidates found by Mróz et al. (2017). Based on their results, Jung et al. (2024) estimated that for KMT-2023-BLG-2669, the Keck host detection probability would be $p \sim 17\%$ at angular lens-source separations of $\Delta\theta \sim 200 \text{ mas}$. Given that our source is similar to that of Jung et al. (2024), we follow the approach used for KMT-2023-BLG-2669, and estimate the detection probability corresponding to our event as $p \sim 16\%$ at $\Delta\theta \sim 200 \text{ mas}$. This suggests that it is difficult to make a distinction between wide-orbit and free-floating planet hypotheses with current telescopes. Nevertheless, because KMT-2024-BLG-3237 is an FFP candidate with the measurement of μ_{rel} , it would be possible to carry out a search for possible hosts within a few years after the event (Jung et al. 2024).

Finally, we note that if the upcoming extremely large telescopes (ELTs) achieve the contrast ratio between the source and the host of $\Delta K \sim 5 \text{ mag}$ at $\Delta\theta = 200 (D/10)^{-1} \text{ mas}$, a putative Sun-like host could be precisely identified in ELTs images taken before the end of the next decade. Here, D is the mirror diameter. For a putative host with $\Delta K \sim 11 \text{ mag}$ (M -type dwarf)¹¹, the wait time will be longer, but it is difficult to make an estimate for this wait time without measuring the performance of ELTs.

¹¹ Hosts have not been identified in the presence of such high contrast ratios, and it is extremely difficult to identify them with current telescopes (see Figure 1 of Mróz et al. 2024).

ACKNOWLEDGMENTS

This research has made use of the KMTNet system operated by the Korea Astronomy and Space Science Institute (KASI) at three host sites of CTIO in Chile, SAAO in South Africa, and SSO in Australia. Data transfer from the host site to KASI was supported by the Korea Research Environment Open NETwork (KREONET). This research was supported by KASI under the R&D program (Project No. 2025-1-830-05) supervised by the Ministry of Science and ICT. H.Y. and W.Z. acknowledge support by the National Natural Science Foundation of China (Grant No. 12133005). H.Y. acknowledge support by the China Postdoctoral Science Foundation (No. 2024M762938). Work by C.H. was supported by the grants of National Research Foundation of Korea (2019R1A2C2085965 and 2020R1A4A2002885).

Table 1. Mean Parameters for FSPL Models

Parameters	FSPL	FSPL ($f_B = 0$)
χ^2/dof	6006.678/6005	6007.374/6006
t_0 (HJD')	541.902 ± 0.003	541.902 ± 0.003
u_0	0.436 ± 0.301	0.465 ± 0.042
t_E (days)	0.561 ± 0.088	0.536 ± 0.018
ρ	1.008 ± 0.265	1.018 ± 0.030
f_S (KMTS41)	0.819 ± 0.410	0.785 ± 0.0001
f_B (KMTS41)	-0.033 ± 0.410	...

NOTE—HJD' = HJD - 2460000

Table 2. Mean Parameters for 2L1S Models

Parameter	Local A	Local B	
		Free f_B	$f_B = 0$
χ^2/dof	6006.237/6002	6000.963/6002	6001.201/6003
t_0 (HJD')	542.041 ± 0.360	541.901 ± 0.004	541.902 ± 0.004
u_0	0.386 ± 0.253	0.309 ± 0.173	0.274 ± 0.048
t_E (days)	0.598 ± 0.074	0.944 ± 0.168	0.929 ± 0.152
s	1.315 ± 0.351	27.987 ± 23.516	30.005 ± 23.727
q (10^2)	$708.051^{+801.884}_{-36.433}$	0.026 ± 0.021	0.021 ± 0.011
α	-0.438 ± 3.241	-0.864 ± 3.437	0.066 ± 3.324
ρ	0.895 ± 0.175	0.624 ± 0.148	0.601 ± 0.084
f_S (KMTS41)	0.661 ± 0.273	1.081 ± 0.829	0.785 ± 0.0001
f_B (KMTS41)	0.124 ± 0.274	-0.296 ± 0.829	...

NOTE—HJD' \equiv HJD - 2460000

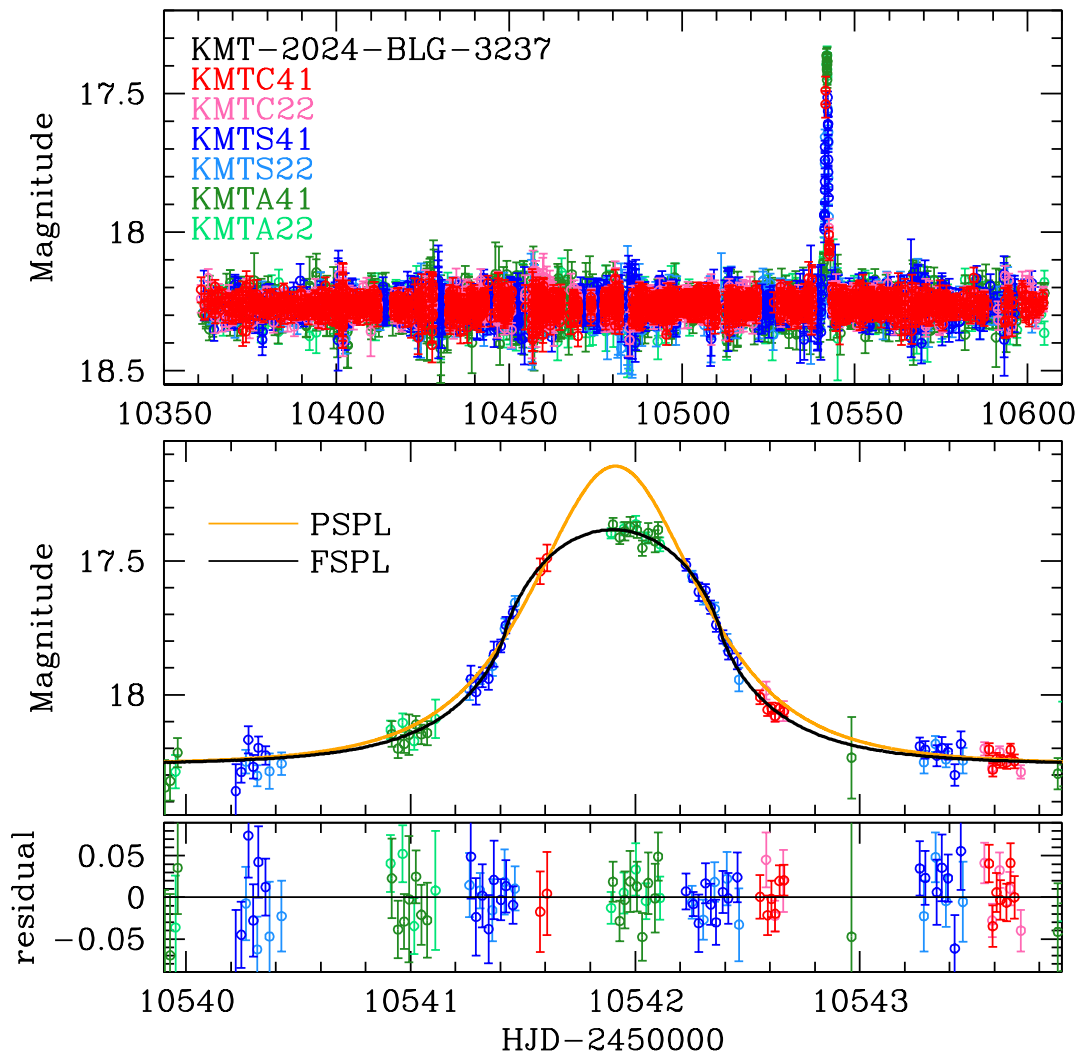


Figure 1. Light curve of KMT-2024-BLG-3237. The upper panel displays the full light curve from the 2024 season, while the lower panel provides the zoom-in of the event. The black and orange curves indicate the FSPL ($f_B = 0$) and the PSPL model, respectively.

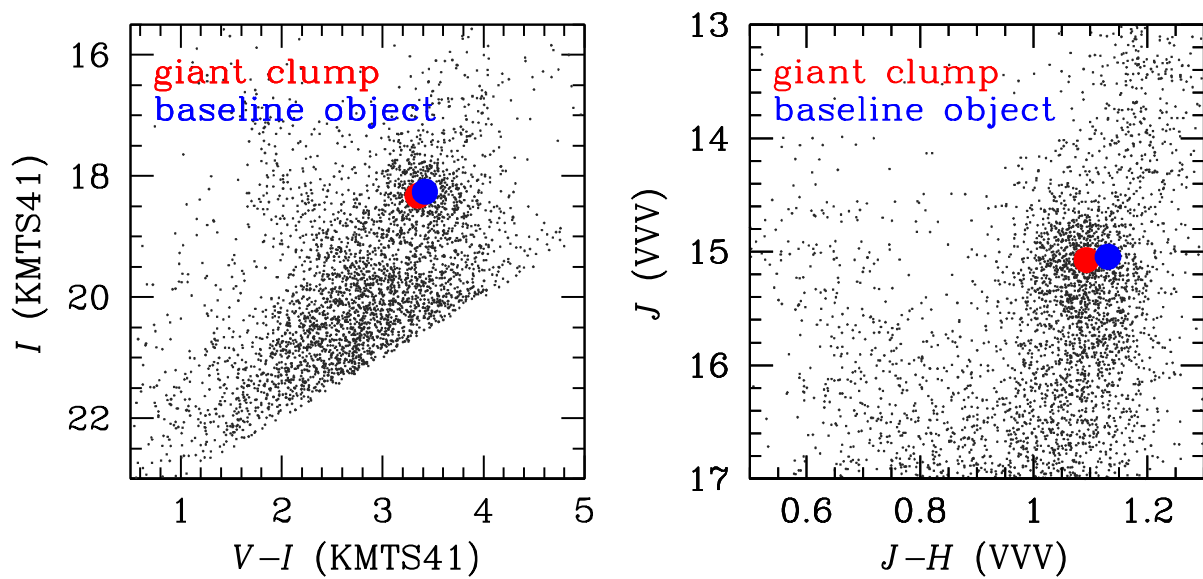


Figure 2. KMTS41 and VVV CMDs for stars in the vicinity (within $4'$) of KMT-2024-BLG-3237. In each panel, the giant clump and baseline object (source) positions are marked by the red and blue dots, respectively.

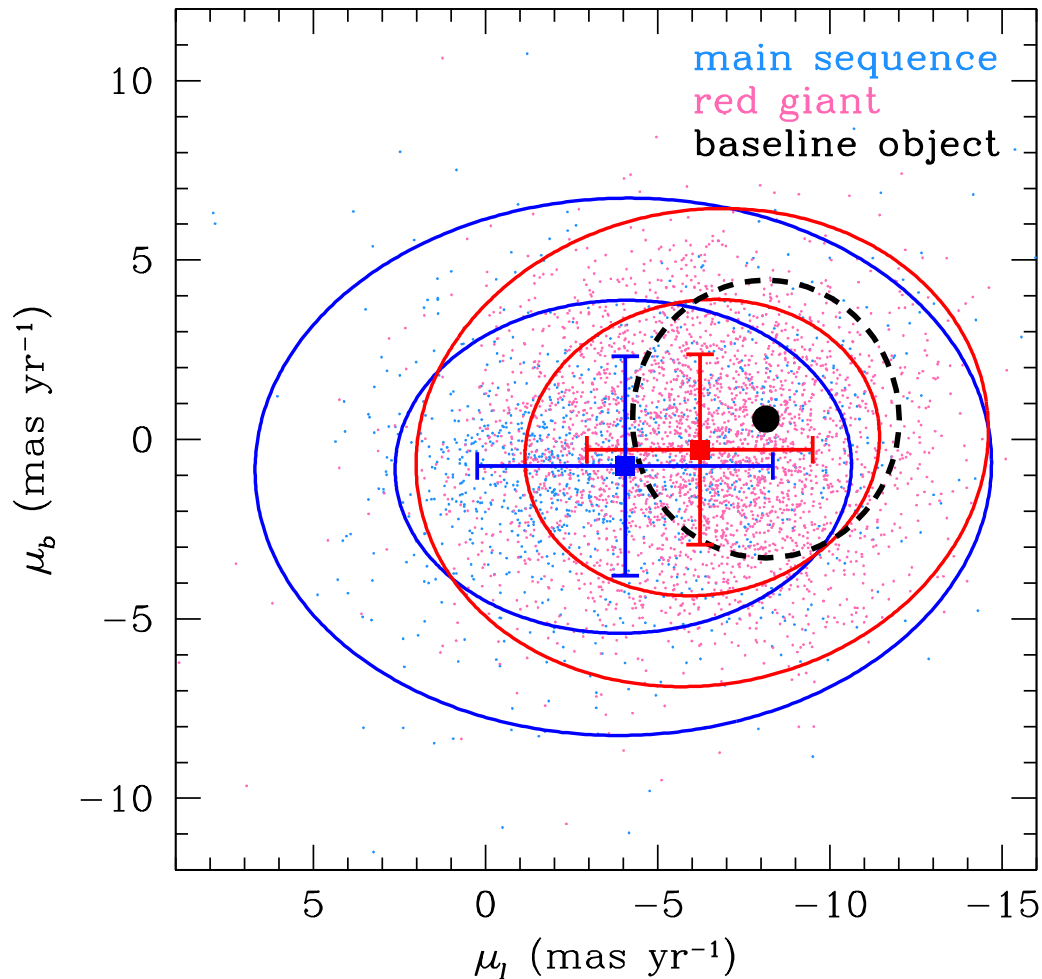


Figure 3. Gaia proper motions of stars in the vicinity (within $6'$) of KMT-2024-BLG-3237. The red dots are red giant (bulge population) stars, while the blue dots are main sequence (disk population) stars. In each population, the inner and outer contours envelope 68% and 95% of the stars, respectively. The red square corresponds to the mean proper motion of the bulge population, $\langle \boldsymbol{\mu}_{\text{bulge}} \rangle (l, b) = (-6.22, -0.29) \pm (3.28, 2.65) \text{ mas yr}^{-1}$. The blue square is the mean proper motion of the disk population, $\langle \boldsymbol{\mu}_{\text{disk}} \rangle (l, b) = (-4.06, -0.74) \pm (4.29, 3.06) \text{ mas yr}^{-1}$. The baseline object (source) is located at the black dot. The black circle represents the locus of the relative lens-source proper motions, $\mu_{\text{rel}} = 4.29 \text{ mas yr}^{-1}$.

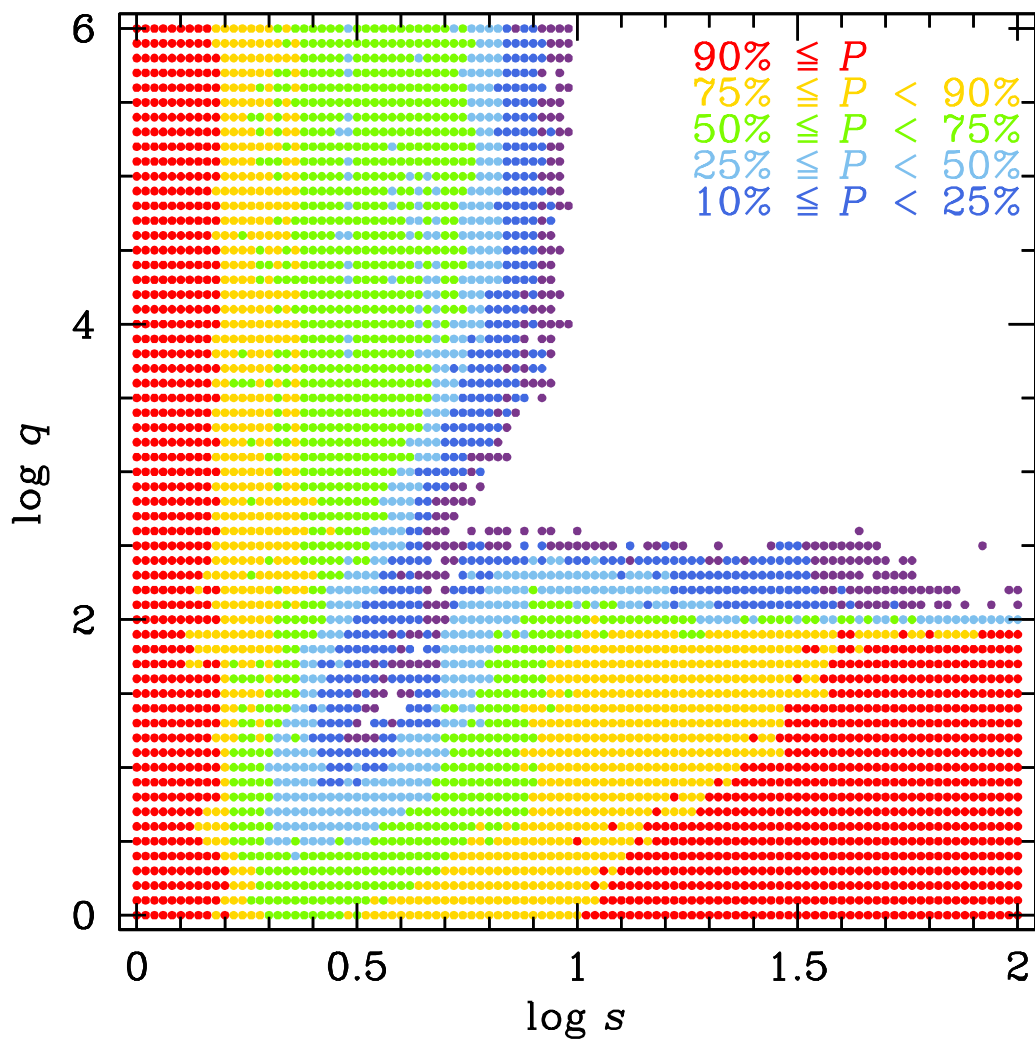


Figure 4. Lens host detection probability in the (q, s) plane.

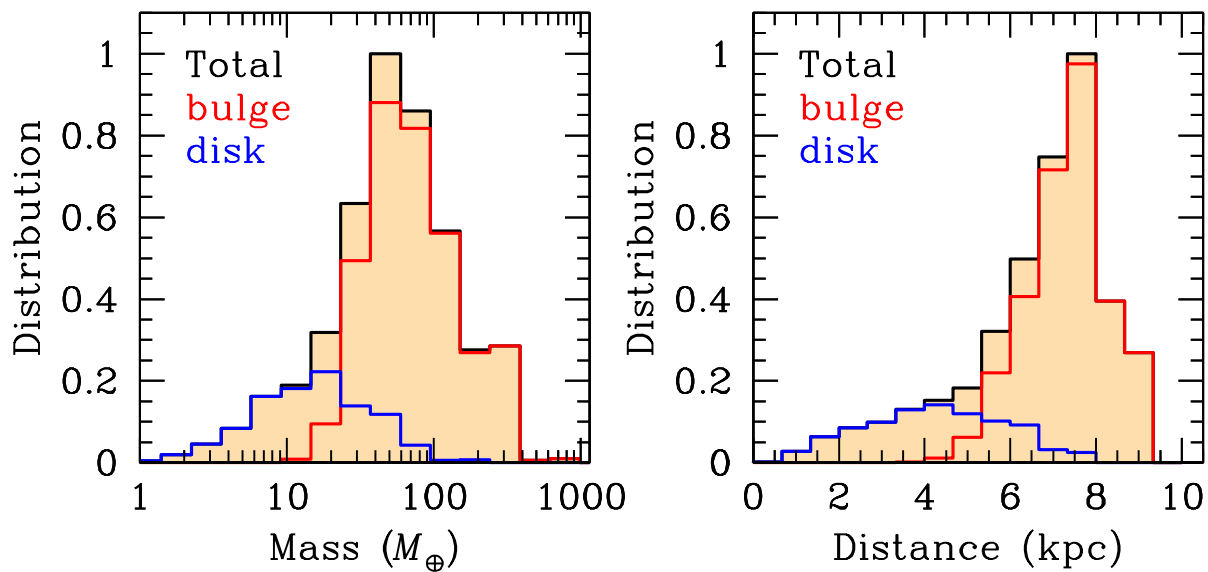


Figure 5. Posterior distributions of M (left) and D_L (right) for KMT-2024-BLG-3237. In each panel, the blue and red distributions correspond to the disk- and bulge-lens contributions, respectively. The black distribution shows the total contribution.

REFERENCES

- Alard, C., & Lupton, R. H. 1998, *ApJ*, 503, 325,
doi: [10.1086/305984](https://doi.org/10.1086/305984)
- Albrow, M. D., An, J., Beaulieu, J.-P., et al. 2001,
ApJ, 549, 759, doi: [10.1086/319437](https://doi.org/10.1086/319437)
- Albrow, M. D., Horne, K., Bramich, D. M., et al.
2009, *MNRAS*, 397, 2099,
doi: [10.1111/j.1365-2966.2009.15098.x](https://doi.org/10.1111/j.1365-2966.2009.15098.x)
- Bachelet, E., Beaulieu, J.-P., Boisse, I., Santerne,
A., & Street, R. A. 2018, *ApJ*, 865, 162,
doi: [10.3847/1538-4357/aad63b](https://doi.org/10.3847/1538-4357/aad63b)
- Ban, M. 2020, *MNRAS*, 494, 3235,
doi: [10.1093/mnras/staa786](https://doi.org/10.1093/mnras/staa786)
- Bennett, D. P., & Rhie, S. H. 1996, *ApJ*, 472, 660,
doi: [10.1086/178096](https://doi.org/10.1086/178096)
- Bensby, T., Yee, J. C., Feltzing, S., et al. 2013,
A&A, 549, A147,
doi: [10.1051/0004-6361/201220678](https://doi.org/10.1051/0004-6361/201220678)
- Bessell, M. S., & Brett, J. M. 1988, *PASP*, 100,
1134, doi: [10.1086/132281](https://doi.org/10.1086/132281)
- Clanton, C., & Gaudi, B. S. 2017, *ApJ*, 834, 46,
doi: [10.3847/1538-4357/834/1/46](https://doi.org/10.3847/1538-4357/834/1/46)
- Claret, A. 2000, *A&A*, 363, 1081
- Gaia Collaboration, Vallenari, A., Brown,
A. G. A., et al. 2023, *A&A*, 674, A1,
doi: [10.1051/0004-6361/202243940](https://doi.org/10.1051/0004-6361/202243940)
- Gaudi, B. S., & Sackett, P. D. 2000, *ApJ*, 528, 56,
doi: [10.1086/308161](https://doi.org/10.1086/308161)
- Gould, A. 1992, *ApJ*, 392, 442,
doi: [10.1086/171443](https://doi.org/10.1086/171443)
- . 1994, *ApJL*, 421, L71, doi: [10.1086/187190](https://doi.org/10.1086/187190)
- . 2000, *ApJ*, 542, 785, doi: [10.1086/317037](https://doi.org/10.1086/317037)
- Gould, A., Carey, S., & Yee, J. 2013, Spitzer
Proposal ID 10036, 10036
- . 2014, Spitzer Proposal ID 11006, 11006
- . 2016, Spitzer Proposal ID 13005, 13005
- Gould, A., Yee, J., & Carey, S. 2015a, Spitzer
Proposal ID 12013, 12013
- . 2015b, Spitzer Proposal ID 12015, 12015
- Gould, A., Yee, J., Carey, S., & Shvartzvald, Y.
2018, Spitzer Proposal ID 14012, 14012
- Gould, A., & Yee, J. C. 2013, *ApJ*, 764, 107,
doi: [10.1088/0004-637X/764/1/107](https://doi.org/10.1088/0004-637X/764/1/107)
- Gould, A., Yee, J. C., & Dong, S. 2024, arXiv
e-prints, arXiv:2406.14531,
doi: [10.48550/arXiv.2406.14531](https://doi.org/10.48550/arXiv.2406.14531)
- Gould, A., Zang, W.-C., Mao, S., & Dong, S.-B.
2021, *Research in Astronomy and Astrophysics*,
21, 133, doi: [10.1088/1674-4527/21/6/133](https://doi.org/10.1088/1674-4527/21/6/133)
- Gould, A., Ryu, Y.-H., Calchi Novati, S., et al.
2020, *Journal of Korean Astronomical Society*,
53, 9. <https://arxiv.org/abs/1906.11183>
- Gould, A., Jung, Y. K., Hwang, K.-H., et al. 2022,
Journal of Korean Astronomical Society, 55,
173, doi: [10.5303/JKAS.2022.55.5.173](https://doi.org/10.5303/JKAS.2022.55.5.173)
- Henderson, C. B., Poleski, R., Penny, M., et al.
2016, *PASP*, 128, 124401,
doi: [10.1088/1538-3873/128/970/124401](https://doi.org/10.1088/1538-3873/128/970/124401)
- Jung, Y. K., Udalski, A., Gould, A., et al. 2018,
AJ, 155, 219, doi: [10.3847/1538-3881/aabb51](https://doi.org/10.3847/1538-3881/aabb51)
- Jung, Y. K., Han, C., Udalski, A., et al. 2021, *AJ*,
161, 293, doi: [10.3847/1538-3881/abf8bd](https://doi.org/10.3847/1538-3881/abf8bd)

- Jung, Y. K., Hwang, K.-H., Yang, H., et al. 2024, *AJ*, 168, 152, doi: [10.3847/1538-3881/ad6b12](https://doi.org/10.3847/1538-3881/ad6b12)
- Kaib, N. A., Raymond, S. N., & Duncan, M. 2013, *Nature*, 493, 381, doi: [10.1038/nature11780](https://doi.org/10.1038/nature11780)
- Kapusta, M., Mroz, P., Ryu, Y.-H., et al. 2025, arXiv e-prints, arXiv:2507.01109, doi: [10.48550/arXiv.2507.01109](https://doi.org/10.48550/arXiv.2507.01109)
- Kervella, P., Bersier, D., Mourard, D., et al. 2004, *A&A*, 428, 587, doi: [10.1051/0004-6361:20041416](https://doi.org/10.1051/0004-6361:20041416)
- Kim, D.-J., Kim, H.-W., Hwang, K.-H., et al. 2018, *AJ*, 155, 76, doi: [10.3847/1538-3881/aaa47b](https://doi.org/10.3847/1538-3881/aaa47b)
- Kim, H.-W., Hwang, K.-H., Gould, A., et al. 2021, *AJ*, 162, 15, doi: [10.3847/1538-3881/abfc4a](https://doi.org/10.3847/1538-3881/abfc4a)
- Kim, S.-L., Lee, C.-U., Park, B.-G., et al. 2016, *Journal of Korean Astronomical Society*, 49, 37, doi: [10.5303/JKAS.2016.49.1.37](https://doi.org/10.5303/JKAS.2016.49.1.37)
- Koshimoto, N., Sumi, T., Bennett, D. P., et al. 2023, *AJ*, 166, 107, doi: [10.3847/1538-3881/ace689](https://doi.org/10.3847/1538-3881/ace689)
- Luhman, K. L. 2012, *ARA&A*, 50, 65, doi: [10.1146/annurev-astro-081811-125528](https://doi.org/10.1146/annurev-astro-081811-125528)
- Malmberg, D., Davies, M. B., & Hogg, D. C. 2011, *MNRAS*, 411, 859, doi: [10.1111/j.1365-2966.2010.17730.x](https://doi.org/10.1111/j.1365-2966.2010.17730.x)
- Minniti, D., Lucas, P., Hempel, M., & The Vvv Science Team. 2023
- Mróz, P., Ban, M., Marty, P., & Poleski, R. 2024, *AJ*, 167, 40, doi: [10.3847/1538-3881/ad1106](https://doi.org/10.3847/1538-3881/ad1106)
- Mróz, P., Udalski, A., Skowron, J., et al. 2017, *Nature*, 548, 183, doi: [10.1038/nature23276](https://doi.org/10.1038/nature23276)
- Mróz, P., Ryu, Y.-H., Skowron, J., et al. 2018, *AJ*, 155, 121, doi: [10.3847/1538-3881/aaaac9](https://doi.org/10.3847/1538-3881/aaaac9)
- Mróz, P., Udalski, A., Bennett, D. P., et al. 2019a, *A&A*, 622, A201, doi: [10.1051/0004-6361/201834557](https://doi.org/10.1051/0004-6361/201834557)
- Mróz, P., Udalski, A., Skowron, J., et al. 2019b, *ApJS*, 244, 29, doi: [10.3847/1538-4365/ab426b](https://doi.org/10.3847/1538-4365/ab426b)
- Mróz, P., Poleski, R., Han, C., et al. 2020a, *AJ*, 159, 262, doi: [10.3847/1538-3881/ab8aeb](https://doi.org/10.3847/1538-3881/ab8aeb)
- Mróz, P., Poleski, R., Gould, A., et al. 2020b, *ApJL*, 903, L11, doi: [10.3847/2041-8213/abfbad](https://doi.org/10.3847/2041-8213/abfbad)
- Nataf, D. M., Gould, A., Fouqué, P., et al. 2013, *ApJ*, 769, 88, doi: [10.1088/0004-637X/769/2/88](https://doi.org/10.1088/0004-637X/769/2/88)
- Nemiroff, R. J., & Wickramasinghe, W. A. D. T. 1994, *ApJL*, 424, L21, doi: [10.1086/187265](https://doi.org/10.1086/187265)
- Park, B. G., DePoy, D. L., Gaudi, B. S., et al. 2004, *ApJ*, 609, 166, doi: [10.1086/420926](https://doi.org/10.1086/420926)
- Pearson, S. G., & McCaughrean, M. J. 2023, arXiv e-prints, arXiv:2310.01231, doi: [10.48550/arXiv.2310.01231](https://doi.org/10.48550/arXiv.2310.01231)
- Rasio, F. A., & Ford, E. B. 1996, *Science*, 274, 954, doi: [10.1126/science.274.5289.954](https://doi.org/10.1126/science.274.5289.954)
- Refsdal, S. 1966, *MNRAS*, 134, 315, doi: [10.1093/mnras/134.3.315](https://doi.org/10.1093/mnras/134.3.315)
- Ryu, Y.-H., Mróz, P., Gould, A., et al. 2021, *AJ*, 161, 126, doi: [10.3847/1538-3881/abd55f](https://doi.org/10.3847/1538-3881/abd55f)
- Shvartzvald, Y., Yee, J. C., Calchi Novati, S., et al. 2017, *ApJL*, 840, L3, doi: [10.3847/2041-8213/aa6d09](https://doi.org/10.3847/2041-8213/aa6d09)
- Sumi, T., Koshimoto, N., Bennett, D. P., et al. 2023, *AJ*, 166, 108, doi: [10.3847/1538-3881/ace688](https://doi.org/10.3847/1538-3881/ace688)

- Tomaney, A. B., & Crotts, A. P. S. 1996, *AJ*, 112, 2872, doi: [10.1086/118228](https://doi.org/10.1086/118228)
- Udalski, A., Yee, J. C., Gould, A., et al. 2015, *ApJ*, 799, 237, doi: [10.1088/0004-637X/799/2/237](https://doi.org/10.1088/0004-637X/799/2/237)
- Veras, D., & Raymond, S. N. 2012, *MNRAS*, 421, L117, doi: [10.1111/j.1745-3933.2012.01218.x](https://doi.org/10.1111/j.1745-3933.2012.01218.x)
- Whitworth, A. P., & Stamatellos, D. 2006, *A&A*, 458, 817, doi: [10.1051/0004-6361:20065806](https://doi.org/10.1051/0004-6361:20065806)
- Witt, H. J., & Mao, S. 1994, *ApJ*, 429, 66, doi: [10.1086/174302](https://doi.org/10.1086/174302)
- Yang, H., Yee, J. C., Hwang, K.-H., et al. 2024, *MNRAS*, 528, 11, doi: [10.1093/mnras/stad3672](https://doi.org/10.1093/mnras/stad3672)
- Yee, J. C., & Kenyon, S. J. 2025, *AJ*, 170, 132, doi: [10.3847/1538-3881/adeb84](https://doi.org/10.3847/1538-3881/adeb84)
- Yee, J. C., Shvartzvald, Y., Gal-Yam, A., et al. 2012, *ApJ*, 755, 102, doi: [10.1088/0004-637X/755/2/102](https://doi.org/10.1088/0004-637X/755/2/102)
- Yee, J. C., Udalski, A., Calchi Novati, S., et al. 2015, *ApJ*, 802, 76, doi: [10.1088/0004-637X/802/2/76](https://doi.org/10.1088/0004-637X/802/2/76)
- Yoo, J., DePoy, D. L., Gal-Yam, A., et al. 2004, *ApJ*, 603, 139, doi: [10.1086/381241](https://doi.org/10.1086/381241)
- Zang, W., Penny, M. T., Zhu, W., et al. 2018, *PASP*, 130, 104401, doi: [10.1088/1538-3873/aadcd3](https://doi.org/10.1088/1538-3873/aadcd3)
- Zhu, W., Udalski, A., Huang, C. X., et al. 2017, *The Astrophysical Journal Letters*, 849, L31, doi: [10.3847/2041-8213/aa93fa](https://doi.org/10.3847/2041-8213/aa93fa)